Electrochemically Triggered Metal–Insulator Transition between VO₂ and V₂O₅

Qiyang Lu, Sean R. Bishop, Dongkyu Lee, Shinbuhm Lee, Hendrik Bluhm, Harry L. Tuller, Ho Nyung Lee, and Bilge Yildiz*

Distinct properties of multiple phases of vanadium oxide (VO$_x$) render this material family attractive for advanced electronic devices, catalysis, and energy storage. In this work, phase boundaries of VO$_x$ are crossed and distinct electronic properties are obtained by electrochemically tuning the oxygen content of VO$_x$ thin films under a wide range of temperatures. Reversible phase transitions between two adjacent VO$_x$ phases, VO$_2$ and V$_2$O$_5$, are obtained. Cathodic biases trigger the phase transition from V$_2$O$_5$ to VO$_2$, accompanied by disappearance of the wide band gap. The transformed phase is stable upon removal of the bias while reversible upon reversal of the electrochemical bias. The kinetics of the phase transition is monitored by tracking the time-dependent response of the X-ray absorption peaks upon the application of a sinusoidal electrical bias. The electrochemically controllable phase transition between VO$_2$ and V$_2$O$_5$ demonstrates the ability to induce major changes in the electronic properties of VO$_x$ by spanning multiple structural phases. This concept is transferable to other multiphase oxides for electronic, magnetic, or electrochemical applications.

1. Introduction

Vanadium dioxide (VO$_2$) has become a focal point of functional oxide research due to its near room-temperature metal–insulator transition (MIT), resulting from a structural phase transition from the rutile VO$_2$(R) to the monoclinic VO$_2$(M1) phase upon cooling through the transition temperature $T_c \approx 340$ K.[1–4] This MIT leads to a drastic change in electrical conductivity of ideally up to five orders of magnitude, promising to enable a variety of new types of oxide electronic devices.[5–8] However, due to the metallic nature of VO$_2$(R) and its high concentration of charge carriers, it is very difficult, if not impossible, to induce the phase transition in the bulk via applying gate voltages with solid-state dielectric materials.[9–11] On the other hand, suppression of the MIT transition below T_c, and reversible control of the electrical conductivity, was achieved by use of an ionic liquid (IL) gate instead of a solid-state dielectric.[12,13] The mechanism behind ionic liquid gating was beyond simple electrostatic polarization or field effect, but instead was electrochemical in nature. The removal of lattice oxygen, leading to reduction of the lattice and creation of oxygen vacancies, was proposed as the source for the suppression of the MIT transition.[14]

In spite of the promise of VO$_2$ as a key component for "more-than-Moore" electronic devices,[15] it has several inevitable shortcomings originating from the character of its MIT. First, the band gap of the insulator phase VO$_2$ (M1) is only ≈0.6 eV,[2,16] which limits the maximum attainable magnitude of device conductance on/off ratios. The achievable on/off ratio of VO$_2$-based devices in single crystal form is ≈10⁵,[17] while this value might be lowered to ≈10³ or even lower for VO$_2$ thin films due to the existence of oxygen nonstoichiometry[1] or cation interdiffusion.[18] This value barely suffices for main stream logic devices requiring on/off ratios of 10³–10⁶[19] and is far lower than ≈10⁷ that is required for low power logic devices (transistors).[20] Moreover, the relatively low T_c of the MIT (≈68 °C) limits the maximum device operation temperature, below which VO$_2$ remains semiconducting. Thus, VO$_2$-based electronic devices may require active cooling to maintain temperature below T_c, thereby imposing additional constraints on deployment.

Dr. Q. Lu,[+] Dr. S. R. Bishop,[++] Prof. B. Yildiz
Laboratory for Electrochemical Interfaces
Massachusetts Institute of Technology
Cambridge, MA 02139, USA
E-mail: byildiz@mit.edu
Dr. Q. Lu, Dr. S. R. Bishop, Prof. H. L. Tuller, Prof. B. Yildiz
Department of Materials Science and Engineering
Massachusetts Institute of Technology
Cambridge, MA 02139, USA

The ORCID identification number(s) for the author(s) of this article can be found under https://doi.org/10.1002/adfm.201803024.

[+]Present address: Oak Ridge National Laboratory, Oak Ridge, TN 37831, USA
[++]Present address: Redox Power Systems, College Park, MD 20742, USA

Dr. D. Lee, Dr. S. Lee, Dr. H. N. Lee
Materials Science and Technology Division
Oak Ridge National Laboratory
Oak Ridge, TN 37831, USA
Dr. H. Bluhm
Chemical Sciences Division
Lawrence Berkeley National Laboratory
1 Cyclotron Road, MS6R2100, Berkeley, CA 94720, USA
Prof. B. Yildiz
Department of Nuclear Science and Engineering
Massachusetts Institute of Technology
Cambridge, MA 02139, USA

In this work, we demonstrate a new pathway to achieve a large range of tunability of the properties in vanadium oxide (VO_x) utilizing the multivalent character of vanadium ions and the multiple phases of vanadium oxides. Vanadium oxides have a rich and complex phase diagram with a correspondingly wide variety of physical properties. Distinct from the existence of the MIT in VO_2, V_2O_5 is an insulting oxide due to the empty 3d orbital, with a wide band gap of ≈2.2 eV.[21] A large modulation in electronic conductivity is therefore achievable by crossing the phase boundary from the metallic $VO_2(R)$ phase (or oxygen-deficient metallic VO_2 phase below T_c, as shown by Jeong et al.[14]) to the insulating V_2O_5 phase. In this paper, we report the electrochemical triggering of a reversible phase transition between the conductive dioxide VO_2 and the insulating pentoxide V_2O_5, accompanied by a reversible metal–insulator transition. This phase transition was obtained by adding/removing oxygen ions via the application of an electrochemical bias.[22–25] This is an electrochemically driven phase transition, similar to our previous study of the $SrCoO_x$ system, that can be switched electrochemically between the layered $SrCoO_{2.5}$ brownmillerite and the $SrCoO_3$ perovskite phase, by application of appropriate electrochemical potentials.[26,27]

To illustrate the feasibility of achieving this electrochemically induced phase transition in VO_x over a wide temperature range, this transition was demonstrated both at 300 °C and at room temperature, on VO_2 thin films of ≈50 nm thick grown on yttria-stabilized zirconia (YSZ) substrates (see **Figure 1**a). At 300 °C, the oxygen ion conducting YSZ serves as a solid electrolyte that enables the pumping of oxygen ions into and out of VO_x films.[24] Ambient pressure X-ray photoelectron spectroscopy and X-ray absorption spectroscopy (AP-XPS/XAS) were performed to probe changes in the VO_x phase, chemical state, and electronic structure as a function of applied electrochemical bias.[24,28] The phase of the thin films was switched from V_2O_5 to VO_2 by applying cathodic electrical biases. AP-XAS of V $L_{2,3}$-edge and O K-edge show the phase boundary between VO_2 and V_2O_5 to be ≈250 mV cathodic bias at $T = 300$ °C and $pO_2 = 200$ mTorr. The valence band (VB) spectra confirmed the change in electronic structure by showing the disappearance of the 2.2 eV band gap when switched from V_2O_5 to VO_2. The phase transition is reversible upon reversing the applied bias, and was cyclable under AC oscillating voltage between 0 and −2 V. Upon removal of the applied bias, the transformed phase was retained in a meta-stable fashion at open circuit conditions, due to the slow kinetics of surface oxygen exchange of VO_x with the gas phase. The reversible phase change obtained at 300 °C, with the VO_x surface exposed to ambient, also made it feasible to perform in operando AP-XAS and XPS measurements that provided a direct and in situ picture of the phase transition and the electronic structure. The $VO_2 \rightarrow V_2O_5$ and the accompanying metal–insulator transition were also triggered at room temperature by use of an ionic liquid as the electrolyte. We found that varying the orientations and thicknesses of VO_2 thin films was important for facilitating the electrochemically triggered phase transition to V_2O_5. The ex situ resistivity measurements on the films switched either at room temperature or at 300 °C demonstrated that the resistivity of the achieved V_2O_5 was significantly higher than the insulating state of VO_2. This study presents a framework for inducing oxygen-controlled phase changes
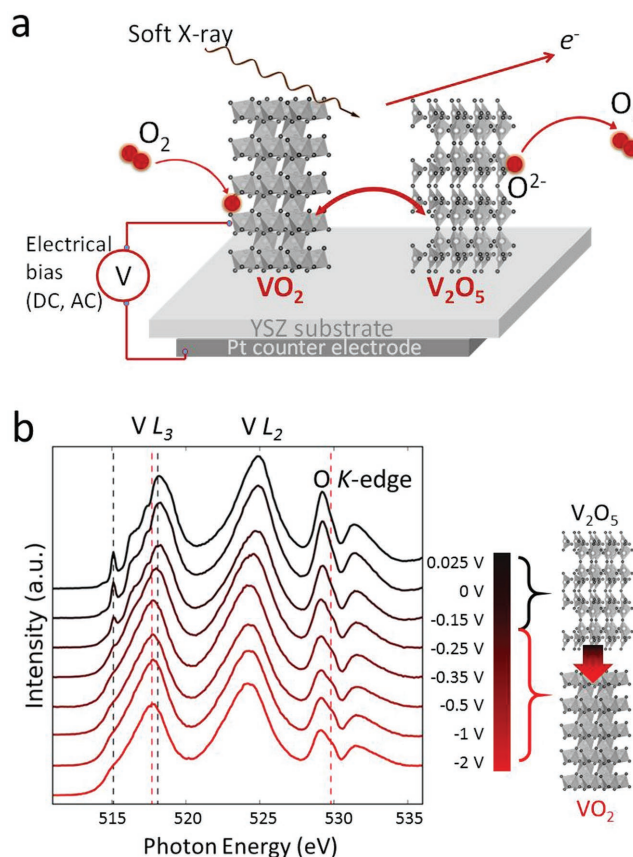

Figure 1. a) Schematic illustration of the ambient pressure X-ray absorption spectroscopy and X-ray photoelectron spectroscopy (AP-XAS, AP-XPS) measurements. Electrical bias was applied onto the VO_x electrode while the absorption and photoelectron spectra were measured in operando. Electrochemical pumping of oxygen out of the film transforms it from V_2O_5 to VO_2, and electrochemical pumping of oxygen into the film transforms VO_2 to V_2O_5. b) AP-XAS data as a function of electrical bias applied to the VO_x/YSZ/Pt electrochemical cell at $T = 300$ °C, $pO_2 = 200$ mTorr. The dashed lines are guides to the eyes that mark changes in the spectral lines in the V $L_{2,3}$-edge and O K-edge designated peaks. The black and red dashed lines mark the V_2O_5 and VO_2 features, respectively. A cathodic bias of −0.25 V triggers the $V_2O_5 \rightarrow VO_2$ transition under these conditions.

in oxides, accompanied by large changes in physical properties, and for revealing the mechanisms and kinetics of these transitions.

2. Results and Discussion

2.1. Resolving the Structure and Phase of VO_x by AP-XAS

AP-XAS measurements provide the opportunity to monitor changes in the crystal structure of VO_x, with the spectra showing clear features indicative of the transition between the layered V_2O_5 and the more closely packed VO_2 structure. In order to monitor the changes in the VO_x crystal and electronic structure, the V $L_{2,3}$-edge (513–527 eV) and O K-edge (527–535 eV) spectra were collected at each bias (Figure 1). The estimated probing depth of these spectra is ≈2 nm (see the Experimental Section). Both spectra changed dramatically as a

function of electrical bias applied to the VO_x working electrode with respect to the platinum (Pt) counter electrode, from 0.025 to −2 V (see Figure 1a). The phase transition boundary occurred at about −0.25 V at $T = 300$ °C, $pO_2 = 200$ mTorr. By comparing the X-ray absorption spectra shape to the reported results in the literature,[2,29] we confirmed that VO_x took on the pentoxide V_2O_5 phase above −0.25 V, while negative electrical biases below −0.25 V triggered the phase transition to the dioxide VO_2. While transitioning from V_2O_5 to VO_2, the main V L_3-edge peak shifted lower by ≈0.6 eV, and the small peak centered at ≈515 eV and the fine structure shoulders of V L_3-edge were gradually suppressed. The extra features in the V L_3-edge of V_2O_5 are from its layered crystal structure, and the small peak and shoulder features can be assigned to the splitting of the unoccupied V 3d orbitals. The presence of these fine structures in the V L_3-edge peak indicates the good crystal quality of V_2O_5; features often absent or are weak when V_2O_5 is amorphous or highly disordered.[29,30] On the contrary, no such features were present in VO_2, which indicated mainly the octahedral splitting to t_{2g} and e_g levels present in the VO_2 phase.

2.2. Change of Electronic Structure and Electrochemical Activity upon Phase Transition

The electrochemically triggered phase transition between V_2O_5 and VO_2 has a substantial impact on both the electronic and electrochemical properties of this oxide system. The drastic change in the electronic structure induced by this phase transition is shown by the VB spectra in **Figure 2**a. The VB spectra were recorded by AP-XPS at $T = 300$ °C, $pO_2 = 200$ mTorr. The VO_2 phase (at an electrical bias of −2 V) under these conditions was metallic, shown by the Fermi edge centered at 0 eV binding energy, consistent with the VB spectra of $VO_2(R)$ reported in the literature.[31] On the other hand, when V_2O_5 was obtained by applying a bias of 0 V, the VB spectrum showed semiconducting characteristics with no states at 0 eV and a valence band maximum at ≈2.2 eV. This proves the existence of the transition from a metal to a wide band-gap insulator state. There exists a large contrast in the electronic structure and conductivity accompanying the phase transition from VO_2 to V_2O_5 solely driven by the electrical control of oxygen stoichiometry.

The change in the electronic structure of VO_x also strongly affects its electrochemical behavior. In the absence of reference electrodes, we characterize the total electrochemical behavior of these cells by examining the steady-state ionic exchange current when an electrical bias is applied. The time dependence of the resulting current upon application of bias provides insights into the electrical changes accompanying the phase change. Figure 2b shows the current relaxation (I–t curve) when an electrical bias step of 0 V →−2 V was applied to V_2O_5, transforming it to VO_2. When an electrical bias is applied

to an electrochemical cell, as in this case consisting of oxide ion conducting YSZ electrolyte and mixed ionic electronic conducting electrodes, one induces the controlled electrochemical pumping of oxygen into or out of the electrode, also known as coulometric titration.[32] Upon full completion of this titration process, the electrical and electrochemical properties of the active material reach a new state and no longer change. During the titration process, the magnitude of current should decay exponentially down to a steady state as the oxygen filling or emptying capacity of the electrodes is reached. However, the I–t curve in Figure 2b shows instead an increase in the magnitude of the current with time, with a relaxation opposite to the normal I–t relaxation behavior associated with coulometric titration. This seemingly odd behavior suggests that the oxygen exchange rate in V_2O_5 is much slower than in VO_2. This is not surprising given that charge transfer between the oxide and adsorbed molecular oxygen is a key rate determining factor impacting the oxygen exchange kinetics.[33,34] The faster oxygen exchange rate on VO_2 compared with that of V_2O_5 can thus be attributed to the much larger concentration of electronic carriers available for charge transfer from VO_2 than from V_2O_5, consistent with changes in electronic structure illustrated in Figure 2a.

2.3. Stability and Cyclability of VO_2 and V_2O_5 Phases

The electrochemically triggered phase transition between VO_2 and V_2O_5 was reversible upon the reversal of the electrical bias on the oxide film. Importantly though, VO_2 and V_2O_5 each remained metastable (kinetically stabilized) after removing the applied electrical bias (i.e., under open circuit) upon achieving the phase transition, owing to the sluggish oxygen exchange kinetics of both phases, even at an elevated temperature of 300 °C. Plots (a) and (c) in **Figure 3** of the X-ray absorption spectra show that both phases were metastable following
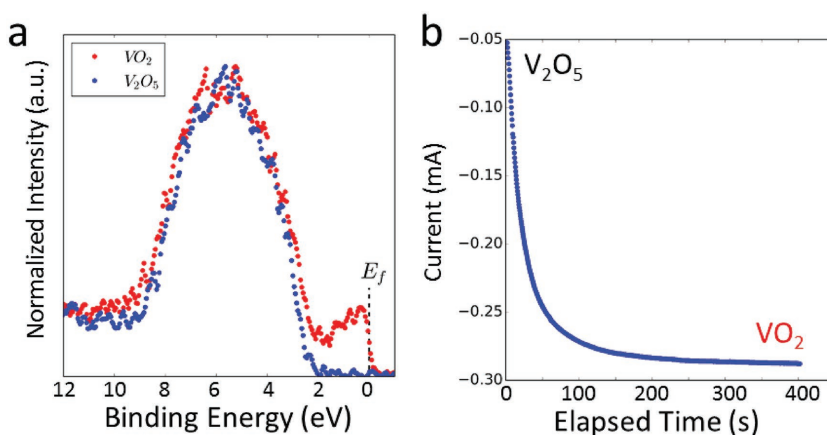

Figure 2. a) Valence band spectra on VO_2 (at an electrical bias of −2 V) and V_2O_5 (at an electrical bias of 0 V) at $T = 300$ °C, $pO_2 = 200$ mTorr. Note that VO_2 is in its metallic rutile phase at the measurement temperature. E_f denotes the position of zero binding energy in the spectrum. b) The current relaxation (I–t curve) when an electrical bias step from 0 to −2 V was applied to V_2O_5 at time = 0 s, transforming it to VO_2. Notice the increase in the current magnitude as a function of time, opposite to the expected decrease of the current magnitude in this oxygen coulometric titration configuration.
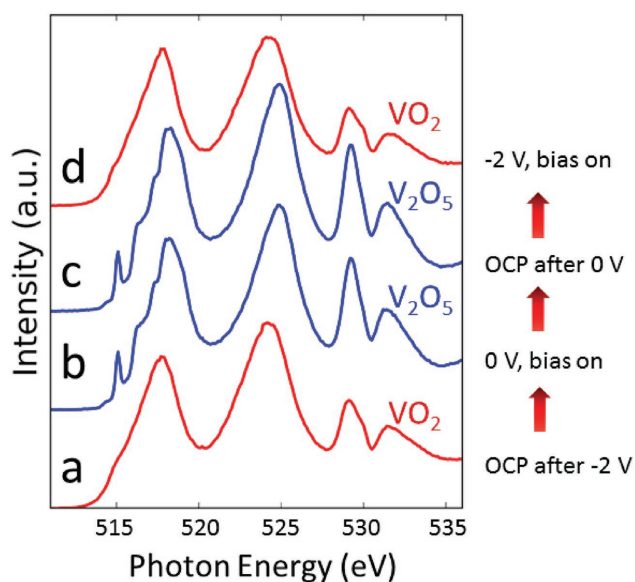
ADVANCED
SCIENCE NEWS
www.advancedsciencenews.com

ADVANCED
FUNCTIONAL
MATERIALS
www.afm-journal.de

Figure 3. X-ray absorption spectra as a function of applied electrical bias and time obtained from the VO_x/YSZ/Pt electrochemical cell maintained at $T = 300\,°C$, $pO_2 = 200$ mTorr. The progression of the experiment indicated by the upward arrows shows the stability and cyclability of the electrochemically triggered phase transition in VO_x. From bottom to top: a) The VO_2 phase was obtained at −2 V, and remained stable after removing the bias and keeping the cell at open circuit potential (OCP) condition. b) As soon as the VO_2 top electrode was shorted to the bottom Pt electrode (setting the electrochemical cell bias to 0 V), the VO_2 changed to the V_2O_5 phase. c) V_2O_5 remained stable after removal of the bias (remained unchanged for 30 min of the measurement). d) An electrical bias of −2 V again switched the V_2O_5 back to VO_2.

removal of the respective applied biases of −2 and 0 V (cell at open circuit potential). The wait time after removing the bias was about 30 min. The phase transition could be reversed when the biases 0 V and −2 V were turned on, as shown by plots (b) and (d). This reversibility and the stability imply that the phase of VO_x (VO_2 or V_2O_5) can be programmed by the application of an electrical bias, creating possible applications for it in novel nonvolatile memory or logic devices.

2.4. Cyclability and Kinetics of Phase Transition Probed by Dynamic X-Ray Absorption Measurements

The cyclability and the kinetics of the electrochemically triggered phase transition were assessed by performing dynamic X-ray absorption measurements. **Figure 4** shows the scheme of such measurements with two measurements at different photon energies. The X-ray absorption spectra of the V_2O_5 and VO_2 phases differ markedly in the V L_3-edge and O K-edge regions (Figure 4a). The excitation photon energy was fixed to selected photon energies, indicated by the red dashed line at 517.7 eV in the V L_3-edge region and by the blue dashed line at 529.2 eV in the O K-edge region. Electrical bias was cycled between 0 and −2 V at the selected photon energies. We could track the periodic change in X-ray absorption intensity at these two photon energies as one periodically transitions between the V_2O_5 and VO_2 phases, shown in Figure 4b. During the

phase transitions between V_2O_5 and VO_2, the X-ray absorption intensities in the V L_3-edge and O K-edge regions change in opposite directions; i.e., when the former increases, the latter decreases and vice versa. As a result, the two dynamic curves in Figure 4b have a phase difference of π.

The dynamic measurements provide us with a means of quantifying the kinetics of the electrochemically triggered phase transition. As shown in Figure 4c, the amplitude of X-ray absorption intensity has a strong dependence on frequency. Lower frequencies (5 mHz) clearly introduce large changes in X-ray absorption, with the maximum and minimum intensities approaching steady state plateaus. Increasing the frequency to 10 mHz or above decreases the achievable amplitude of the X-ray absorption intensity difference. At 100 mHz, no appreciable periodic change in X-ray absorption intensity can be observed. This means that the phase transition kinetics cannot keep up with the rate of voltage change at such high frequencies. This observed frequency dependence can be well explained by the kinetics of the phase transitions. Oxygen ion transport in the YSZ electrolyte and oxygen ion transfer at the YSZ/VO_x interfaces are precursors to the phase transition between VO_2 and V_2O_5 in this cell. All of these reactions each have respective time constants. Especially the oxygen transport through the YSZ substrate of macroscopic dimensions is very slow. At lower frequency such as 5 mHz, the voltage rate of change was slow enough to complete the phase transition, yielding a correspondingly large observed absorption change. An upper limit for the time constant (for this geometry of the electrochemical cell) can be estimated from Figure 4c. Selecting 1/4 of the period of the 5 mHz curve that exhibits the plateau gives an upper limit of ≈50 s for the time constant of the reaction. On the contrary, at faster frequencies there is insufficient time for the phase transition to fully complete, leading to decreased amplitudes as plotted in Figure 4c. One can also deduce from Figure 4c that the oxidization step ($VO_2\rightarrow V_2O_5$) is slower than the reduction step ($V_2O_5\rightarrow VO_2$). This is consistent with the faster oxygen incorporation kinetics in VO_2 compared with V_2O_5, as is already demonstrated by Figure 2b and the related discussion.

2.5. Electrochemically Triggered Metal–Insulator Transition at Room Temperature

The AP-XAS/XPS measurements performed at 300 °C with the aid of the electrochemical cell utilizing a YSZ solid electrolyte enabled a thorough analysis of the crystal and electronic structural changes that accompany the voltage-induced phase transitions in VO_x. Given that these transitions are driven by electrochemical control of the oxygen content within these oxide films, they do not necessarily require the use of elevated temperatures. It should be noted that the slow kinetics of transition shown above even at 300 °C is also limited by the very slow oxide ion transport across the YSZ electrolyte whose ionic conductivity is strongly thermally activated.[35] In order to demonstrate that this switching process is feasible at ambient temperatures, we resort to gating the VO_x film with an ionic liquid (IL) instead of YSZ as the oxygen ion conducting electrolyte. We used 1-hexyl-3-methylimidazoliumbis (trifluoromethylsulfonyl)-imide (HMIM-TFSI) IL since it reportedly supports relatively fast oxygen transport at room temperature.[14] We found that
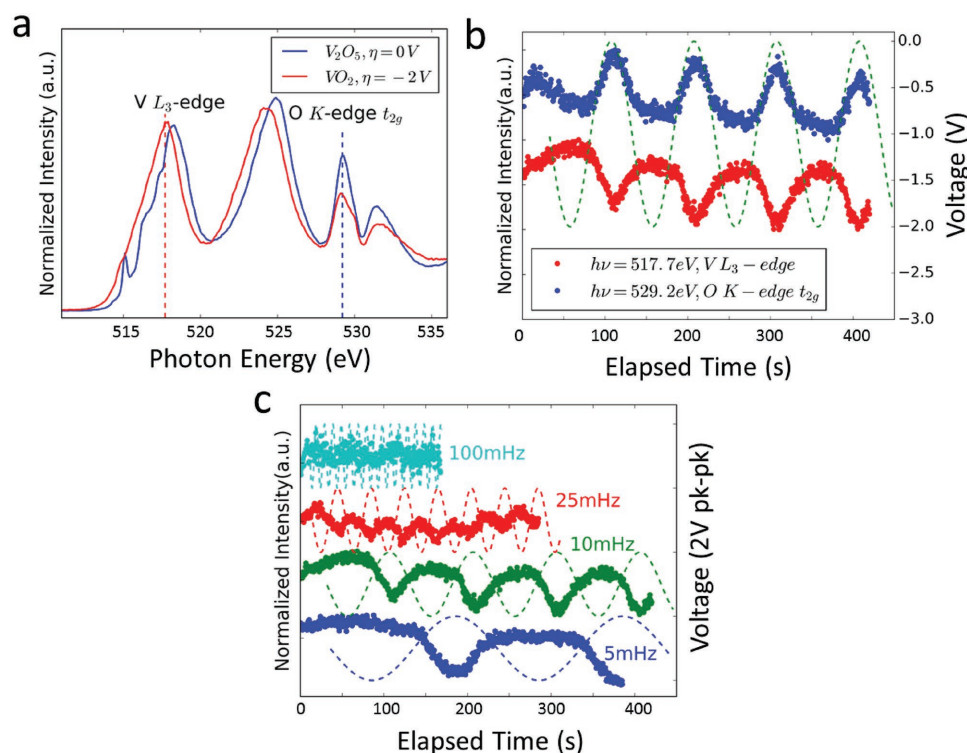
Figure 4. Dynamic X-ray absorption measurements. a) The V $L_{2,3}$-edge and O K-edge regions of the X-ray absorption spectra at 0 and −2 V obtained from the VO_x layer as part of the VO_x/YSZ/Pt electrochemical cell operating at $T = 300$ °C, $pO_2 = 200$ mTorr. V_2O_5 is stabilized at 0 V and VO_2 at −2 V. The dashed lines mark the two photon energies (517.7 and 529.2 eV) where large changes in the X-ray absorption intensity exist when switching from one phase to the other. b) Applied sine wave electrical bias (green dashed line) with a frequency of 10 mHz, and the corresponding periodic changes of X-ray absorption intensity at the two selected photon energies in the V L_3-edge region at 517.7 eV (red data points) and in the O K-edge region at 529.2 eV (blue data points). Note that the two curves are ≈180° out of phase. c) Frequency-dependency of the dynamic X-ray absorption intensity at $h\nu = 517.7$ eV in the V L_3-edge region, measured during cycling of the electrical bias applied to the VO_x/YSZ/Pt electrochemical cell at several frequencies (5, 10, 25, and 100 mHz) with a peak-to-peak variation of 2 V as in (b). At 5 mHz the absorption intensity reached plateaus both under 0 and −2 V applied bias, with the amplitude of X-ray absorption intensity gradually decreasing with increasing frequency.

two factors are important in the feasibility of $VO_2 \rightarrow V_2O_5$ phase transition at room temperature. These are the orientation and the thickness of the VO_2 thin film, with the (001) orientation and a smaller thicknesses being favorable. The VO_2(100)/YSZ thin films could not be electrochemically switched completely to V_2O_5 by using IL, beyond a thin surface layer. This is possibly because of the more close-packed (100) facets, which can block the pathways for oxygen incorporation and slower oxygen diffusion in this direction. Using the (001) orientation on the other hand, with a VO_2(001)/TiO_2 sample, we found that the film thickness of 15.7 nm was too thick, and only showed a very small effect after ionic liquid gating at 4 V. We speculate that the oxygenation might be limited to the near-surface region in this case, due to the sluggish kinetics of oxygen incorporation and diffusion at room temperature (RT). Therefore, electrochemically triggered phase transition at room temperature was successful using a thinner film of 5.7 nm thick VO_2(001) on TiO_2(001). On this thin film, an electrical bias of 4 V applied on the IL-gated cell configuration (Figure S6, Supporting Information) triggered the phase transition from VO_2 to V_2O_5 at room temperature. The phase transition was confirmed by measuring the oxidation state of vanadium (**Figure 5**a) and the valence band spectra (Figure 5b) by ex situ lab-source XPS, following removal of the ionic liquid. The V 2p and VB spectra

obtained after 4 V polarization through the ionic liquid were very similar to the data collected in situ by AP-XPS while transformed from VO_2 to V_2O_5. As seen in Figure 5b, the V 3d states at the Fermi level (0 eV binding energy) disappeared after IL gating, and this proves the metal–insulator transition induced by electrochemical biasing. The V $2p_{2/3}$ peak after IL gating was similar to the V_2O_5 data obtained in situ by AP-XPS under an electrical bias of 25 mV. The narrower width of the peak in AP-XPS data might be from the much smaller photon energy dispersion of synchrotron radiation. Both the more oxidized V state as seen by V $2p_{2/3}$ and the lack of states at Fermi level prove that VO_2 was transformed to V_2O_5 at room temperature within the probing depth of the lab-source XPS (estimated as ≈6 nm). Since the probing depth of XPS was roughly the same as the thickness of the VO_x thin film, we could assume the XPS data represented the whole thin film bulk. This was also validated by X-ray diffraction (XRD) and transport measurement data. XRD results (**Figure 6**a) showed that VO_2 was grown epitaxially on the TiO_2(001) single crystal substrate. The VO_2 diffraction peak was suppressed after ionic liquid gating, indicating the phase transition to V_2O_5. Transport measurements (Figure 6b) showed that the metal–insulator transition in temperature space disappeared after gating with ionic liquid. The gated sample remained insulating up to the highest
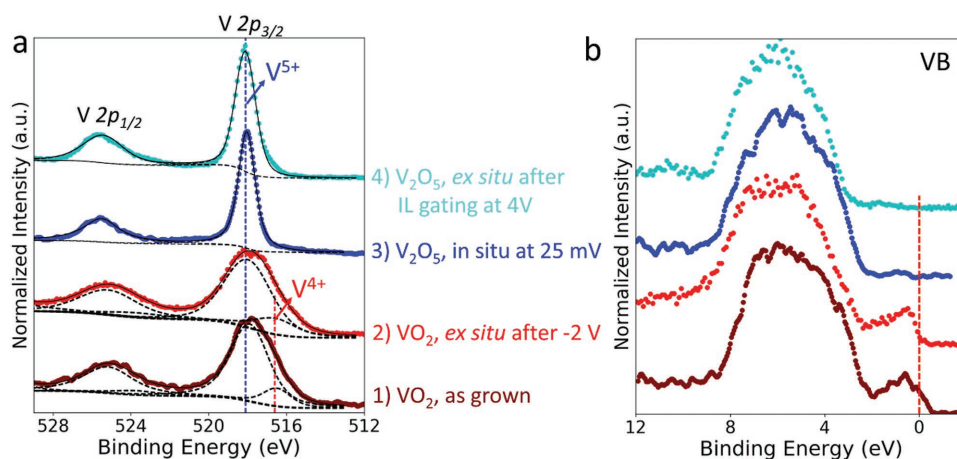
Figure 5. X-ray photoelectron spectra of a) V 2p and b) valence band (VB) before and after ionic liquid (IL) gating, compared with AP-XPS results. 1 and 3) In situ AP-XPS measurements under applied electrical biases of −2 V and 25 mV, which corresponds to VO$_2$ and V$_2$O$_5$ phases, respectively. 2) Ex situ XPS on as-grown VO$_2$(001)/TiO$_2$(001) thin film. The XPS data at this state were similar to the in situ AP-XPS data on VO$_2$. 4) VO$_2$(001)/TiO$_2$(001) after ionic liquid gating at 4 V. The V 2p peak was similar to the in situ AP-XPS spectrum under 25 mV, while the V 3d states at 0 eV binding energy disappeared, confirming the transformation to the insulating V$_2$O$_5$ phase. The dashed lines in (a) are the XPS peak fitting results showing the contribution of different oxidation states (V^{5+} and V^{4+}), similar to the AP-XPS analysis shown in Figure S4 in the Supporting Information. While the V 2p$_{3/2}$ spectra in 3) and 4) can be fitted with a single peak, indicating the fully oxidized V^{5+} chemical state, the spectra in 1) and 2) consist of two peaks, corresponding to the mixed V^{5+} and V^{4+} states.

measurement temperature. The new phase had much higher resistivity compared to the insulating VO$_2$ phase below the MIT transition temperature of VO$_2$. Figure S5 (Supporting Information) shows the XRD and the resistance obtained on the VO$_2$(010)/YSZ and after it was switched to V$_2$O$_5$ at 300 °C and cooled to room temperature. The resulting electronic features are qualitatively similar to the comparison presented in Figure 6, and the XRD peaks obtained after switching are consistent with the V$_2$O$_5$ phase. The resistivity of the electrochemically obtained V$_2$O$_5$ thin films (in Figure 6 and Figure S5, Supporting Information) falls within the range of resistivities reported for V$_2$O$_5$ thin films in the literature.[1] Most importantly, the electrochemically switched V$_2$O$_5$ thin films here do not exhibit any metal-to-insulator transition as a function of temperature, consistent with V$_2$O$_5$ electronic properties. The drastic changes in electronic structure and electrical

conductivity, obtained electrochemically here over a wide range of temperatures, might open new pathways of utilizing the multiphase character of VO$_x$ in novel oxide electronic devices.

3. Conclusion

In summary, phase transitions between VO$_2$ and V$_2$O$_5$ were obtained by electrochemical control of oxygen content within the VO$_x$ film. Upon removal of the electrical bias, the obtained phases remain metastable (kinetically stabilized) due to the slow oxygen gas exchange kinetics at the measurement temperatures used in this study (room temperature and 300 °C). The valence band spectra and current relaxation curves demonstrated the drastic changes in electronic and electrochemical properties accompanying the phase transition between VO$_2$ and
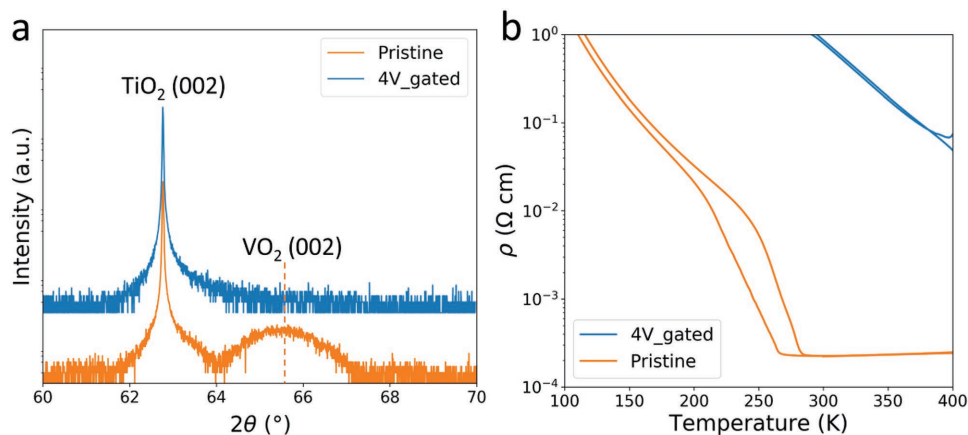

Figure 6. a) X-ray diffraction results on pristine (as-grown) and 4 V gated VO$_2$/TiO$_2$(001) thin films. The pristine film showed the VO$_2$(002) diffraction peak. After ionic liquid gating, the VO$_2$(002) peak disappeared. b) Transport measurement showing the temperature-dependent resistivity of pristine and gated VO$_2$/TiO$_2$(001).

V_2O_5. Measured periodic changes in X-ray absorption intensity, induced under an applied sinusoidally varying cell voltage, enabled observation of cyclability of the phase transitions. By use of ionic liquid gating, it was possible to demonstrate the ability to induce this metal–insulator transition electrochemically even under ambient conditions. One can make a distant analogy to phase change resistive memories;[36] however, the clear distinction and advantage here is that the phase change is obtained by electrochemical control of composition, rather than by heating. The changes in phase and electronic structure were possible to observe by macroscopic probes of XPS and XAS. The results demonstrate the ability to actively tune and design ionic defects in electronic oxides in a powerful enough manner to be able to cross phase boundaries to obtain distinct physical properties. This electrochemically controlled phase change based MIT, between the metallic VO_2 and the insulating V_2O_5, has the potential for a much larger conductance on/off ratio, a higher resistance in the off state, and extended operation temperature regimes. These findings have implications for design of novel devices taking advantage of the distinctly different electrical, optical, and electrochemical properties of the multiple possible phases of vanadium oxide.

4. Experimental Section

VO_x Thin Film Growth: Epitaxial VO_2 thin films were grown on single crystal (001) YSZ substrates using pulsed laser epitaxy (PLE). PLE growth of VO_2 films was conducted at 450 °C and 7 mTorr of oxygen. The laser fluence and repetition rate were fixed at 1 J cm^{-2} and 10 Hz, respectively. In order to ensure the correct oxygen stoichiometry, as-grown VO_2 thin films were cooled to 300 °C and annealed for 10 min under an oxygen partial pressure of 100 Torr. (see ref. [4] of the main text for more details on PLE of VO_2 thin films.) Prior to VO_2 deposition, Pt counter electrodes were painted on one side of the YSZ and treated at 900 °C in air for 1 h. The YSZ substrate was fixed to the PLE substrate holder using a small amount of silver paint for thermal contact. The samples were structurally characterized with high-resolution four-circle XRD (X'Pert, Panalytical Inc.); see Figure S1 in the Supporting Information for structural characterizations.

AP-XPS/XAS: AP-XPS/XAS was carried out at Beamline 11.0.2, Advanced Light Source, Lawrence Berkeley National Laboratory. The VO_2/YSZ thin film sample was placed on a customized sample holder with a button ceramic heater. Porous Pt was used at the backside of the YSZ substrate as the counter electrode with characteristically rapid oxygen reduction and evolution reactions. A piece of Pt foil was placed in between the heater and VO_2 thin film sample, contacting the Pt counter electrode. K-type thermocouples were fixed on the sample surface with a ceramic piece and clips, also holding a small piece of Au foil, which served as top electrode. A Biologic SP-300 potentiostat was used to apply electrochemical bias and perform chronoamperometric measurements. For XPS measurements, V 2p and O 1s core levels, as well as valence band spectra, were collected using a photon energy hv of 735 eV. The estimated inelastic mean free path is ≈0.8 nm. The XAS measurements were performed using the partial electron yield (PEY) method. The electron kinetic energy window for V $L_{2,3}$-edge and O K-edge XAS was 350 ± 20 eV. We estimate the probing depth of the PEY-XAS to be comparable or lower than the mean probing depth of total-electron-yield XAS reported in the literature, which is ≈2 nm.[37] Care was taken to minimize possible beam damage. The photon shutter was kept closed between measurements, while the sample was always moved to a new area before each measurement. Under this condition, no noticeable beam damage was observed within the timespan of the measurements (see Figure S2, Supporting Information).

IL Gating: IL HMIM-TFSI was used as an oxygen ion conducting electrolyte at room temperature. It is believed believe that different ILs should behave similarly in serving as the liquid electrolyte gate according to the systematic survey of IL effects in previous studies.[14] An electrical bias was applied between the VO_x and the gate electrode for ≈30 min until the measured current stabilized, using a cell configuration as shown in Figure S4 (Supporting Information). Then the IL was removed and the VO_x sample was thoroughly rinsed with isopropanol and acetone. A lab source XPS (PHI-5500 ESCA Spectrometer with monochromated Al Kα (1486.65 eV) X-ray radiation, equipped with charge neutralization, was used to monitor the chemical state of vanadium before and after IL gating.

Supporting Information

Supporting Information is available from the Wiley Online Library or from the author.

Conflict of Interest

The authors declare no conflict of interest.

[1] S. Lee, T. L. Meyer, S. Park, T. Egami, H. N. Lee, *Appl. Phys. Lett.* **2014**, *105*, 223515.

[2] S. Lee, T. L. Meyer, C. Sohn, D. Lee, J. Nichols, D. Lee, S. S. A. Seo, J. W. Freeland, T. W. Noh, H. N. Lee, *APL Mater.* **2015**, *3*, 126109.

[3] M. M. Qazilbash, M. Brehm, B. G. Chae, P.-C. Ho, G. O. Andreev, B. J. Kim, S. Y. Yun, A. V. Balatsky, M. B. Maple, F. Keilmann, H. T. Kim, D. N. Basov, *Science* **2007**, *318*, 1750.

[4] N. B. Aetukuri, A. X. Gray, M. Drouard, M. Cossale, L. Gao, A. H. Reid, R. Kukreja, H. Ohldag, C. A. Jenkins, E. Arenholz, K. P. Roche, H. A. Durr, M. G. Samant, S. S. P. Parkin, *Nat. Phys.* **2013**, *9*, 661.

**ADVANCED
SCIENCE NEWS**

www.advancedsciencenews.com

**ADVANCED
FUNCTIONAL
MATERIALS**

www.afm-journal.de

[5] M. Brahlek, L. Zhang, J. Lapano, H.-T. Zhang, R. Engel-Herbert, N. Shukla, S. Datta, H. Paik, D. G. Schlom, *MRS Commun.* **2017**, *7*, 27.

[6] D. Li, A. A. Sharma, D. K. Gala, N. Shukla, H. Paik, S. Datta, D. G. Schlom, J. A. Bain, M. Skowronski, *ACS Appl. Mater. Interfaces* **2016**, *8*, 12908.

[7] N. Shukla, A. V Thathachary, A. Agrawal, H. Paik, A. Aziz, D. G. Schlom, S. K. Gupta, R. Engel-Herbert, S. Datta, *Nat. Commun.* **2015**, *6*, 7812.

[8] T. Driscoll, H.-T. Kim, B.-G. Chae, B.-J. Kim, Y.-W. Lee, N. M. Jokerst, S. Palit, D. R. Smith, M. Di Ventra, D. N. Basov, *Science* **2009**, *325*, 1518.

[9] M. Belyaev, A. Velichko, P. Boriskov, N. Kuldin, V. Putrolaynen, G. Stefanovitch, *J. Sel. Top. Nano Electron. Comput.* **2014**, *2*, 26.

[10] S. Sengupta, K. Wang, K. Liu, A. K. Bhat, S. Dhara, J. Wu, M. M. Deshmukh, *Appl. Phys. Lett.* **2011**, *99*, 2.

[11] D. Ruzmetov, G. Gopalakrishnan, C. Ko, V. Narayanamurti, S. Ramanathan, *J. Appl. Phys.* **2010**, *107*, 114516.

[12] M. Nakano, K. Shibuya, D. Okuyama, T. Hatano, S. Ono, M. Kawasaki, Y. Iwasa, Y. Tokura, *Nature* **2012**, *487*, 459.

[13] H. Ji, J. Wei, D. Natelson, *Nano Lett.* **2012**, *12*, 2988.

[14] J. Jeong, N. Aetukuri, T. Graf, T. D. Schladt, M. G. Samant, S. S. P. Parkin, *Science* **2013**, *339*, 1402.

[15] Y. Zhou, S. Ramanathan, *Proc. IEEE* **2015**, *103*, 1289.

[16] D. Fu, K. Liu, T. Tao, K. Lo, C. Cheng, B. Liu, R. Zhang, H. A. Bechtel, J. Wu, *J. Appl. Phys.* **2013**, *113*, 1.

[17] L. A. Ladd, W. Paul, *Solid State Commun.* **1969**, *7*, 425.

[18] H. Paik, J. A. Moyer, T. Spila, J. W. Tashman, J. A. Mundy, E. Freeman, N. Shukla, J. M. Lapano, R. Engel-Herbert, W. Zander, J. Schubert, D. A. Muller, S. Datta, P. Schiffer, D. G. Schlom, *Appl. Phys. Lett.* **2015**, *107*, 1.

[19] K. Kim, J.-Y. Choi, T. Kim, S.-H. Cho, H.-J. Chung, *Nature* **2011**, *479*, 338.

[20] *Int. Technol. Roadmap Semicond. (ITRS)* **2015**, https://www.semiconductors.org/main/2015_international_technology_roadmap_for_semiconductors_itrs/.

[21] S. Krishnakumar, C. S. Menon, *Phys. Stat. Solidi A* **1996**, *153*, 439.

[22] J. Walter, H. Wang, B. Luo, C. D. Frisbie, C. Leighton, *ACS Nano* **2016**, *10*, 7799.

[23] P. P. Orth, R. M. Fernandes, J. Walter, C. Leighton, B. I. Shklovskii, *Phys. Rev. Lett.* **2016**, *106801*, 1.

[24] D. N. Mueller, M. L. Machala, H. Bluhm, W. C. Chueh, *Nat. Commun.* **2015**, *6*, 6097.

[25] M. Setvín, U. Aschauer, P. Scheiber, Y.-F. Li, W. Hou, M. Schmid, A. Selloni, U. Diebold, *Science* **2013**, *341*, 988.

[26] Q. Lu, B. Yildiz, *Nano Lett.* **2016**, *16*, 1186.

[27] Q. Lu, Y. Chen, H. Bluhm, B. Yildiz, *J. Phys. Chem. C* **2016**, *120*, 24148.

[28] N. Tsvetkov, Q. Lu, L. Sun, E. J. Crumlin, B. Yildiz, *Nat. Mater.* **2016**, *15*, 1010.

[29] C. W. Zou, Y. F. Rao, A. Alyamani, W. Chu, M. J. Chen, D. A. Patterson, E. A. C. Emanuelsson, W. Gao, *Langmuir* **2010**, *26*, 11615.

[30] E. Goering, O. Müller, M. Klemm, M. L. DenBoer, S. Horn, *Philos. Mag. Part B* **1997**, *75*, 229.

[31] T. C. Koethe, Z. Hu, M. W. Haverkort, C. Schüßler-Langeheine, F. Venturini, N. B. Brookes, O. Tjernberg, W. Reichelt, H. H. Hsieh, H. J. Lin, C. T. Chen, L. H. Tjeng, *Phys. Rev. Lett.* **2006**, *97*, 1.

[32] J. Maier, *Phys. Chem. Ionic Mater.: Ions Electrons in Solids* **2004**, *1*.

[33] W. Jung, H. L. Tuller, *Adv. Energy Mater.* **2011**, *1*, 1184.

[34] Y. Chen, Z. Cai, Y. Kuru, W. Ma, H. L. Tuller, B. Yildiz, *Adv. Energy Mater.* **2013**, *3*, 1221.

[35] N. P. Brandon, S. Skinner, B. C. H. Steele, *Annu. Rev. Mater. Res.* **2003**, *33*, 183.

[36] S. Raoux, W. Welnic, D. Lelmini, *Chem. Rev.* **2010**, *110*, 240.

[37] M. Abbate, J. B. Goedkoop, F. M. F. de Groot, M. Grioni, J. C. Fuggle, S. Hofmann, H. Petersen, M. Sacchi, *Surf. Interface Anal.* **1992**, *18*, 65.

1803024 (8 of 8)